Biochimica et Biophysica Acta 1800 (2010) 655–661

Contents lists available at ScienceDirect

Biochimica et Biophysica Acta

journal homepage: www.elsevier.com/locate/bbagen

AFM observation of single, functioning ionotropic glutamate receptors reconstituted in lipid bilayers

Nahoko Kasai [a,*], Chandra S. Ramanujan [b], Ichiro Fujimoto [c], Akiyoshi Shimada [a], John F. Ryan [b], Keiichi Torimitsu [a]

[a] NTT Basic Research Laboratories, NTT Corporation, Kanagawa, Japan
[b] Department of Physics, University of Oxford, Oxford, UK
[c] The Institute of Medical Science, University of Tokyo, Tokyo, Japan

ARTICLE INFO

Article history:
Received 26 November 2009
Received in revised form 11 February 2010
Accepted 4 March 2010
Available online 20 March 2010

Keywords:
AMPA receptor
Atomic force microscopy
Membrane protein
Neuroreceptor

ABSTRACT

Background: Ionotropic glutamate receptors (iGluRs) are responsible for extracellular signaling in the central nervous system. However, the relationship between the overall structure of the protein and its function has yet to be resolved. Atomic force microscopy (AFM) is an important technique that allows nano-scale imaging in liquid. In the present work we have succeeded in imaging by AFM of the external features of the most common iGluR, AMPA-R (α-amino-3-hydroxy-5-methyl-4-isoxazole propionic acid receptor), in a physiological environment.
Methods: Homomeric GluR3 receptors were over-expressed in insect cells, purified and reconstituted into lipid membranes. AFM images were obtained in a buffer from membranes immobilized on a mica substrate.
Results: Using Au nanoparticle-conjugated antibodies, we show that proteins reconstitute predominantly with the N-terminal domain uppermost on the membrane. A tetrameric receptor structure is clearly observed, but it displays considerable heterogeneity, and the dimensions differ considerably from cryo-electron microscopy measurements.
Conclusions: Our results indicate that the extracellular domains of AMPA-R are highly flexible in a physiological environment.
General significance: AFM allows us to observe the protein surface structure, suggesting the possibility of visualizing real time conformational changes of a functioning protein. This knowledge may be useful for neuroscience as well as in pharmaceutical applications.

1. Introduction

Glutamate is an excitatory neurotransmitter in the mammalian central nervous system that transfers signals among neurons via synapses and is therefore critical to neuronal networks in terms of memory and learning. After being released from presynaptic terminals, glutamate binds to and activates receptors located on the post-synaptic membrane, thereby transmitting signals. Glutamate receptors can be classified into two categories: ligand-gated ion-channel receptor proteins, iGluRs, and the metabotropic receptors, mGluR, which are G-protein coupled receptors. Among the iGluR, the allosteric AMPA-R mediates fast synaptic neurotransmission by opening its channel briefly, depolarizing the postsynaptic membrane and generating a receptor potential, i.e. neuronal firing [1]. This evoked potential stimulates *N*-methyl-D-aspartate receptors, another type of iGluRs, to permeate potassium, sodium and calcium ions thereby mediating slow neurotransmission and inducing synaptic plasticity [2]. Dysfunction of AMPA-Rs is implicated in various neurological disorders such as epilepsy, stroke, Alzheimer's and Parkinson's diseases, and Huntington's chorea. Thus, the antagonists of this receptor are thought to be effective pharmacological agents in preventing neuronal degeneration associated with glutamate excitotoxity. In fact, there are several reports of the competitive AMPA-R antagonists as therapeutic agents for neuroprotection [3], epilepsy [4], schizophrenia [5], encephalomyelitis [6] and migraine [7].

AMPA-R consists of four subunits, GluR1-4, which form an ion-channel whose function depends on the subunit composition [8,9]. For example, subunit composition regulates synaptic trafficking [10] as well as subunit recruitment [11]. The activation of ligand-gated ion channel receptors involves conformational changes within each subunit which open the channel and allow permeation of cations so mediating fast synaptic transmission.

Abbreviations: AFM, atomic force microscopy; iGluR, ionotropic glutamate receptor; AMPA-R, α-amino-3-hydroxy-5-methyl-4-isoxazole propionic acid receptor; cryo-EM, cryo-electron micrograph; SDS-PAGE, sodium dodecyl sulfate-polyacrylamide gel electrophoresis; WGA, wheat germ agglutinin; DEAE, diethylaminoethyl

* Corresponding author. NTT Basic Research Laboratories, 3-1 Morinosato Wakamiya, Atsugi, Kanagawa, 243-0198 Japan. Tel.: +81 46 240 3535; fax: +81 46 270 2364.
E-mail address: nahoko@nttbrl.jp (N. Kasai).

0304-4165/$ – see front matter © 2010 Elsevier B.V. All rights reserved.
doi:10.1016/j.bbagen.2010.03.002

Each AMPA-R subunit consists of an amino-terminal domain (NTD), two ligand-binding domains (LBD), and a transmembrane domain (TMD) [12,13]. Structural studies have concentrated mostly on the ligand-binding domain using electrophysiology [14] and X-ray crystallography [15–17]. Rosenmund et al. inferred that AMPA-R is tetrameric from the step-like increase in single-channel conductance observed in the presence of a saturating concentration of agonist [18]. Ayalon and Stern-Bach found that the tetramer was formed as a dimer-of-dimers, and later showed that the first dimer assembly is mediated by interactions between compatible NTDs [19]. In subsequent investigations Sobolesky et al. [20] found evidence suggesting that the 2-fold rotational symmetry of the ligand-binding domains extends down to the extracellular vestibule of the channel, with a possible transition to 4-fold rotational symmetry occurring deeper within the pore.

Cryo-electron microscopy (cryo-EM) of single intact AMPA-Rs (at 2 nm resolution) also indicates that the receptor may have a dimer-of-dimers configuration; it measures $17 \times 11 \times 14$ nm, with the largest dimension corresponding to longitudinal extent along the two-fold symmetry axis [21,22]. Another group found that the AMPA-R conformation changed by the stimulation, and that the orientation of NTDs also changes substantially by desensitization [23].

While cryo-EM can image the whole intact protein, it does not allow structural measurements under physiological conditions. Atomic force microscopy (AFM), on the other hand, permits sub-molecular resolution imaging in a liquid environment [24]. Single RNA polymerase [25] and membrane proteins [24] have been imaged using AFM under physiological conditions to reveal features with sub-nm resolution. We have recently succeeded in visualizing the ligand-gated ion channel inositol 1,4,5-triphosphate receptor (IP3-R), a large tetrameric membrane protein located on the endoplasmic reticulum, using AFM in aqueous conditions [26].

In the present study we have used AFM to observe the structure of the functioning homomeric iGluR which contains only GluR3 subunits. Although most of the AMPA-Rs in the brain are heteromeric [9], we chose the GluR3 homomer to simplify the receptor activity and reduce the complexity. We reconstituted purified AMPA-R into artificial lipid bilayers in order to maintain its structure and biological activity by establishing conditions similar to those in the native membrane. Channel activity was confirmed using electrophysiological assays. We then examined the orientation of the reconstituted protein using antibody reactions, and finally we imaged the structure of the single, isolated receptors.

2. Materials and methods

2.1. Purification

We used High Five insect cells to overexpress iGluR, which is reported to be preferable to *spodoptera frugiperda* (Sf21) because of lower aggregation and higher yield [21]. GluR3 was purified using ultracentrifugation and affinity columns as described in a previous report [27]. In brief, ~ 10^8 cells insect cells were homogenized using a Potter-type homogenizer in a homogenate buffer with protease inhibitor (Roche Ltd, Basel Switzerland), then the membrane fraction obtained by ultracentrifugation (Beckman Coulter, CA, USA) was solubilized. The soluble membrane fraction was purified first with agarose wheat germ agglutinin (WGA)-Sepharose CL4B (2 ml, Vector Laboratories Inc., CA, USA), then with diethylaminoethyl (DEAE)-Sepharose CL6B (2.5x32cm, Amersham Bioscience, Little Chalfont, UK). The final protein content was 8.4 and 12.8 μg/ml in the most concentrated fractions.

The purified sample was analyzed by sodium dodecyl sulfate polyacrylamide gel electrophoresis (SDS-PAGE) with silver staining (Wako, Osaka, Japan), and by western blotting using the rabbit anti-GluR2/3 antibody (Chemicon, MA, USA) with HRP conjugated anti-rabbit IgG antibody (Jackson Immuno Research Laboratories, West Grove, USA).

2.2. Electrophysiology

The activity of the purified protein was determined using a conventional patch clamp amplifier (Axopatch 200B) and data acquisition system (Digidata 1440A) (both from Molecular Devices, Sunnyvale, USA) based on the painting method described previously [28]. In brief, the inner and outer chambers were separated by a polyvinyl chloride membrane with a 200 μm diameter hole. Both chambers were filled with the measurement solution: 100 mM NaCl, 5 mM KCl, 2 mM $CaCl_2$, 10 mM Tris–HCl (pH 7.4). Lipid solution (phosphatidylcholine from egg yolk: phosphatidylserine from porcine brain = 3:1, 20 mg/ml in decane, both from Avanti, Alabaster, USA) was placed over the cis (inner chamber) side of the hole and immediately immersed into the measurement solution. Ag/AgCl electrodes were used to monitor the current between the outer and inner chambers. After confirming a giga-ohm resistance of the lipid membrane on the hole, protein solution was applied carefully via a glass capillary positioned just above the lipid membrane from the trans side, and the current was monitored at a sampling rate 10 kHz. AMPA and CNQX were used for stimulation and inhibition respectively.

2.3. Reconstitution

The protein solution was mixed with 2.0 % detergent, *n*-ctyl-D-glucopyranoside (Sigma, St. Louis, USA), and with a mixed lipid solution (same components as used in the electrophysiological measurement) for 10 min. After stabilizing for 10 min at room temperature, the solution was dialyzed with a 12–14 k MWCO cellulose membrane (Spectrum, Gardena, USA) for at least 72 h at 4 °C against Buffer A (30 mM HEPES HCl (pH 7.4), 5 mM EDGA, 1 mM EGTA, NaN_3 0.02%). Molecular ratio of lipid-protein was 100,000 to 1.

2.4. Atomic force microscopy

The reconstituted protein was placed on a freshly cleaved mica substrate and kept for 30 min at room temperature before observation. AFM (Dimension 3100™, Digital Instruments Veeco Metrology, Woodbury, USA) measurements were made in tapping mode in buffer solution (30 mM HEPES (pH7.4), 260 mM KCl and 40 mM NaCl) using silicon nitride cantilevers with pyramidal tips (TR800PSA, Olympus, Tokyo, Japan). Small cantilevers with a length of 100 μm and spring constant of 0.57 N/m were used for all measurements. The pixel resolution was 256 × 256 to make sure we scanned quite quickly – typical scan rate was 2 Hz. The imaging force setpoint had a peak at around 2 nN. Image analysis was performed using SPIP (Scanning Probe Image Processor, Image Metrology, Horsholm, Denmark) and Illustrator (Adobe, San Jose, USA).

2.5. Antibody determination of protein orientation

Receptor orientation in the membrane was determined by AFM through the observation of Au nanoparticles attached to the receptors using the following antibody protocol:

(i) Mouse anti-GluR3 antibody (immunogen: GluR3 N-terminus peptide) (Chemicon), followed by anti-mouse IgG conjugated with 10 nm Au particles (Sigma);
(ii) Rabbit anti-GluR2/3 antibody (immunogen: GluR3 C-terminus peptide (EGYNVYGIESVKI, Chemicon), anti-rabbit IgG conjugated with 10 nm gold (Sigma).

The reconstituted sample was allowed to stabilize on the mica for 40 min, then washed with Buffer A, after which the 20-times-diluted first antibody solution was applied for 90 min at room temperature. Then, after thoroughly washing with Buffer A, the 10-times-diluted Au nanoparticle-attached second antibody was applied for 120 min at

room temperature. The sample was then observed with AFM as described above.

3. Results

3.1. Purified protein

Western blotting and silver staining of SDS-PAGE measurements of the purified protein are shown in Fig. 1. Lanes W1 through W5 indicate the western blotting results obtained after WGA column purification; D1 and D2 show the results obtained after DEAE column purification, the final step in the purification process. Samples numbered W1 through W5 were mixed and further purified using the DEAE column. Silver staining data are also shown for D1 and D2 samples. The results showed obvious bands near 100 kDa that correspond to GluR3 (100373 Da, accession number: NP_16785). Using anti-GluR3 antibody we also confirmed the band of the same molecular weight when we purified the protein from rat brain. Silver staining results showed no obvious proteins coexisting in the final sample. Thus SDS-PAGE with immunostaining and the silver staining results verified that the protein is highly purified.

3.2. Electrophysiology

We determined that the channel activity of the AMPA-R was consistent with that of purified GluR3 using the electrophysiological method described above. After an artificial lipid bilayer formed over the 200 μm aperture, the membrane current was recorded using a 1 kHz low pass filter. A voltage step of either 40 mV or −80 mV was applied as shown in Fig. 2(A) and (D). At 40 mV, no obvious current spikes were observed except for the capacitive current (Fig. 2(B)), while at −80 mV, multiple current spikes were observed (Fig. 2(E)). When the antagonist CNQX (1 μM) was present before the AMPA was added, the spikes were completely extinguished as shown in Fig. 2(C) and (F). When the membrane potential is held at negative voltages, the receptor exhibits inward rectification, and when the membrane potential is positive, the receptor does not conduct. These results are consistent with previous observations that AMPA-Rs display rectification characteristics when they do not contain the GluR2 subunit [29]. The observation that all the current spikes are in one direction demonstrates that the AMPA-R incorporated into the artificial lipid bilayer with the extracellular domain to the trans-side and the intracellular domain to the cis-side.

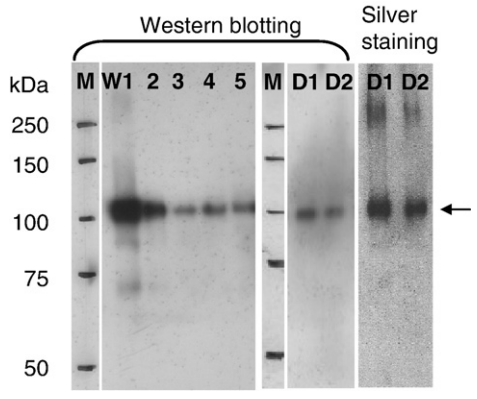

Fig. 1. SDS-PAGE results of the purified AMPA-R: western blotting, and silver staining. W1 to W5 show the results obtained after WGA column purification; D1 and D2 show results obtained after DEAE column purification – the final samples. Samples taken from W1 through W5 were mixed and further purified using the DEAE column. The arrow shows the band at molecular weight of ~100 kDa, which corresponds to GluR3, the homomeric AMPA-R used in this study.

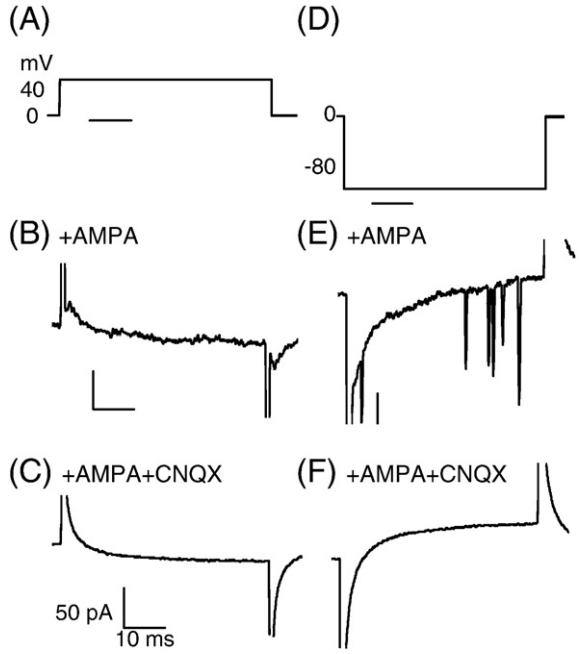

Fig. 2. Electrical measurements of AMPA-R activity in an artificial lipid bilayer. The voltage step was either 40 mV (A) or −80 mV (D), and the current was recorded in the presence of either AMPA (Sigma Aldrich) (B, E) or AMPA with CNQX (6-cyano-7-nitroquinoxaline-2,3-dione, Tocris Bioscience) (C, F) for 40 mV step (B, C) and −80 mV step (E, F). The concentrations of AMPA and CNQX were 290 nM and 1 μM, respectively.

3.3. AFM images

Fig. 3 shows AFM images of the protein sample obtained after purification (Fig. 3(A)), and then after reconstitution in a supported lipid bilayer (Fig. 3(B)). Fig. 3(A) shows a number of ~100 nm lipid domains (red arrows), which arise from the small amount of lipid used in the final process of purification. Fig. 3(A) also shows large speck-like features 60–70 nm diameter (blue arrows) which correspond to aggregated proteins. These features were located mostly at the edge of the membrane patches. We decided to avoid such features because they are not uniformly supported by the membrane, and instead we concentrated our AFM studies on proteins that lie well away from the edge of the membrane.

After reconstitution the lipid patches were much more extensive than in the purified samples: Fig. 3(B) shows a large lipid domain greater than 1 μm in extent. Many features are evident in the interior of the domains as indicated by the arrows. More importantly, smaller features were more abundant after reconstitution as shown by green arrows. This suggests that the reconstitution process tends to separate the aggregated proteins to assume a more stable configuration as isolated molecules within the lipid membrane. The large features, shown by the blue arrows, indicate where proteins aggregated, possibly due to not being reconstituted successfully. To achieve a stable reconstituted sample, careful determination of the ratio of lipid-to-protein ratio and detergent was required.

Fig. 3(C) and (D) show the height profiles measured along the white scan lines indicated in each image. These measurements show that the height of the lipid domain is 4~5 nm above the mica substrate. The thickness of the C16:0/C18:1 phosphatidylcholine lipid bilayer is reported to be 3.5 nm [30]. This height difference is due to the trapped water layer located between the bilayer and the mica substrate which has been previously estimated to be 1–2 nm [9,31].

3.4. Protein identification by antibody attachment

After successful reconstitution, we confirmed the protein as AMPA-R by monitoring antibody reactions to the samples. Fig. 4

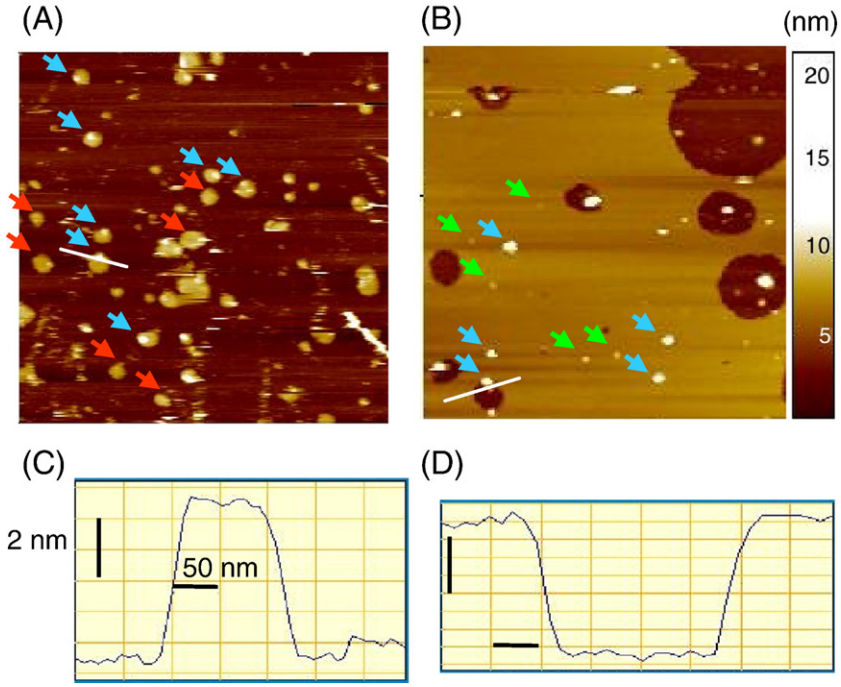

Fig. 3. AFM images (2×2 μm) of AMPA-R: (A) after purification; (B) after reconstitution into the artificial lipid bilayer. The blue arrows indicate large features, green arrows indicate smaller features. Panels C and D are height profiles measured along the white scan lines indicated in the inset AFM images. The black bars indicate 2 nm for the vertical direction and 50 nm for the horizontal direction. (A): lipid domain sizes were about 100 nm, the smaller features were located mostly on the edge of the patches. (B) Large domains, with small features located in the middle. Panels C and D show the lipid domains, with the lowest part corresponding to the mica surface.

shows close-up AFM images of two different positions in the same sample before and after treatment. Fig. 4(A) shows a topographic image of reconstituted protein before the introduction of antibodies, while Fig. 4(B) shows the image obtained after antibody reaction. Fig. 4(C) and (D) plot the height profiles obtained along the scan lines indicated by the white lines. Before antibody reactions the lateral dimension of the features is approximately 40 nm and the height is ~2 nm above the bilayer (Fig. 4(A)); after antibody reactions the feature sizes are 60–80 nm across and 6–8 nm in height (Fig. 4(B)). This increase in the feature size indicates that the 10 nm Au particle-conjugated antibody is attached, thereby confirming the identity of the protein.

The variations in feature size observed after antibody reaction may have several contributions. First, there may be more than one antibody attached to each receptor, because the AMPA-R contains four GluR3 subunits. Also, the Au nanoparticles conjugated IgG exist in a range of diameters 4.9–13.5 nm, the mean value being 7.8 nm. It is energetically more favorable for the smaller Au-IgG nanoparticles to bind to the first antibody [32,33] which may account for the observed height increase being less than 10 nm. Other studies have also found that the Au nanoparticles are easily removed from the antibodies [34], in which case only the attached antibodies would contribute to any change in feature height.

3.5. Orientation of the reconstituted proteins

We investigated the orientation of the reconstituted protein using antibodies that attach either to the N-terminal domain on the extracellular side of the membrane or to the C-terminal on the cytoplasmic side. The basis of the method relies on measuring height changes in the structure by AFM after antibody attachment.

Fig. 5 shows the height distribution of the proteins observed in reconstituted lipid domains (2×2 μm image size, n = 9 images). In Fig. 5 (A), the red bars indicate results obtained before antibody reactions; the blue bars show data obtained after the reaction with the N-terminal antibody and the green bars show heights measured after the C-terminal antibody reaction. Both antibody reactions were followed by an Au particle-conjugated secondary antibody reaction as described above. The curves in Fig. 5(B) show fitted Gaussian distributions. When the N-terminal antibody was used, the occurrence of the features with

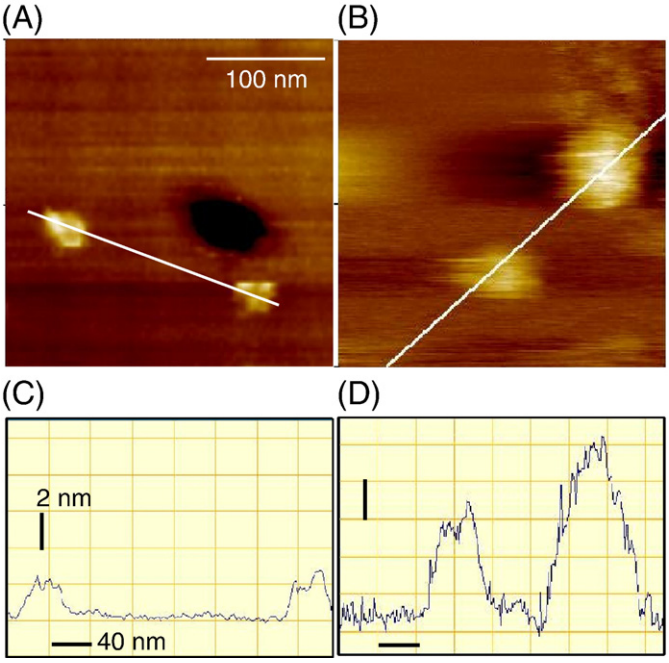

Fig. 4. AFM images and cross-sectional profiles of reconstituted AMPA-R proteins: (A) before, and (B) after antibody reactions. The protrusions correspond to proteins and the flat domain is the surface of the lipid bilayer. The white scale bars in the image indicate 100 nm. Panels C and D are height profiles measured along the white scan lines indicated in the inset AFM images. The black scale bars are 2 nm for vertical and 40 nm for horizontal directions. Features increased in both height and lateral extent by the antibody reaction, indicating that the Au particle-conjugated secondary antibodies were attached to the features.

heights in the range 1.5–2.5 nm above the membrane disappeared. On the other hand, after the C-terminal antibody reaction, features with heights 1.0–1.5 nm disappeared. In both cases we observe a significant increase in features with heights in the range 7–16 nm. A *t*-test statistical analysis of the data gave significant differences for both smaller (1–6 nm) ($P<0.1$) and higher (7–16 nm) ($P<0.005$) height features for N-terminal antibody data. From the Gaussian curves, the height changes resulting from N-terminal antibody attachment were about 1 nm or 6 nm as shown by the dotted arrows in Fig. 5(B). However, C-terminal antibody data did not give significant differences; the data in fact show that only a small proportion of the proteins increased in height, much smaller than the proportion showing a height change after N-terminal antibody attachment. These results indicate that features with height 1.5–2.5 nm correspond to the N-terminal domain being presented on top of the supported membrane (distal to the mica substrate). Smaller features may correspond to the C-terminal being oriented uppermost, but this will require further data to provide confirmation.

The change in height histogram (Fig. 5) shows that the N-terminal antibody changed the histogram more significantly than the C--terminal antibody, demonstrating that the domains lying above the lipid bilayer were predominantly NTDs. This result is not surprising because the extracellular domain consisting of the NTD and LBD is relatively large, more than 700aa, while C-terminal domain is about 40aa. Therefore, when reconstituted, it would be energetically unfavorable for N-terminal to be inserted into lipid vesicles, whereas the C-terminal would readily insert. When the vesicles rupture onto the mica surface, the lower part of the vesicle would rupture and inner leaflet of the lipid bilayer would lie on the mica while outer leaflet would lie uppermost and be exposed to the AFM probe. In this way the N-terminal could be observed by AFM with higher probability than the C-terminals.

The height shift resulting from the N-terminal antibody reaction as indicated in the height histogram was about 1 nm and 6 nm (shown as arrows in Fig. 5(B)). The 6 nm height shift indicates that the Au particle attached to the protein was smaller than the nominal value of 10 nm. This could due to the size distribution of the Au nanoparticles as mentioned previously. The antibodies with smaller Au nanoparticles could be sterically easy to move and bind more readily to the protein [32,33]. This may also due to that only the first antibody attaches to the protein and that second antibody does not attach as the antibody dimensions are reported to be similar to 6 nm [35].

We also observed some proteins became larger than 14 nm after the antibody reaction (Fig. 5(A)). This might be the size of the both first and second antibodies including Au nanoparticles, or the both first and second antibodies without Au nanoparticles because there was a report that Au nanoparticles will detach from the antibodies by degeneration [34].

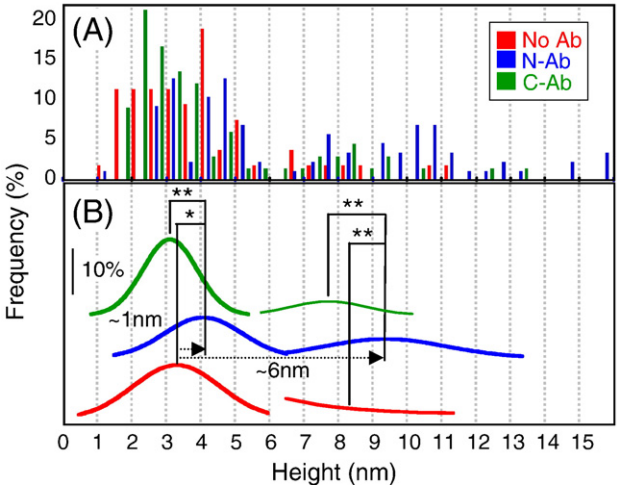

Fig. 5. Height histograms of the AMPA-R proteins before and after the antibody reactions. (A) Red columns show the result with no antibody reaction. Blue columns show the result obtained after reaction to NTD-antibodies, and green columns show the results obtained with C-terminal antibodies. Both antibody reactions were followed by reaction to the secondary antibody attached with a gold nanoparticle. (B) The curves correspond to fitted Gaussian distributions. Red curves were obtained before antibody reaction, blue curves were obtained after N-terminal antibody reaction, and green curves after C-terminal antibody reaction. The results of significant difference examined by *t*-test are indicated as * ($P<0.01$) and ** ($P<0.005$). On addition of the antibody for N-terminal, features with height in the range 1.5~2.5 nm disappeared and features higher than 7~16 nm increased. The C-terminal antibody did not give significant difference in the height histogram. These results imply that the features with height 1.5~2.5 nm correspond mainly to AMPA-Rs reconstituted with N-terminal topmost on the bilayer. ($n=60$–70 for each condition.)

3.6. AMPA-R structure

We observed 49 particles in 18 preparations using 12 cantilevers. Fig. 6 presents high-resolution AFM images of the extracellular surface of the reconstituted AMPA-R. These images reveal features with height ~ 2 nm of approximately the same overall size but with a range of shapes. In some cases a distinct tetrameric internal structure is resolved, which corresponds to the four NTD sub-units. The height of the domains above the membrane is substantially smaller than the length of the combined NTD and LBD measured by cryo-EM (~10 nm), whereas the mean diameter (~16 nm) is larger than the mean width observed in the cryo-EM measurements [23]. In the cryo-EM studies the proteins were isolated from any surrounding membrane by detergents and then frozen. The difference in protein environment might therefore be expected to give rise to differences in size, especially as the AFM measurements come closer to physiological conditions, but AFM tip-induced deformation may also be a contributing factor.

4. Discussion and conclusions

The results presented here show that functioning AMPA-R has been successfully expressed, purified and reconstituted into supported lipid membranes. Consistent with expectations, there is a preferred protein orientation which arises from its highly asymmetric form: a large hydrophilic extracellular domain versus the much smaller cytoplasmic domain, which strongly biases the direction of insertion into the membrane. The AFM studies using Au-nanoparticle-attached antibodies provide clear confirmation of this preferred orientation. Electrophysiology measurements demonstrate that the protein is functional when inserted in a planar lipid membrane; it is reasonable to conclude that it remains functional when reconstituted in supported lipid membranes, although confirmation of this would require, for example, simultaneous electrical and AFM measurements [36]. In the absence of agonist in the imaging buffer we can conclude that the receptor is present in the inactivated state for all the AFM measurements.

The AFM data provide direct evidence of a tetrameric protein structure, although the marked structural heterogeneity evident in Fig. 6 does not permit a definite identification of the proposed dimer-of-dimers subunit configuration. The images of individual membrane-bound receptors presented in Fig. 6 are quite different from the AFM images of two-dimensional protein crystals (see e.g. [24]) which display a highly homogeneous protein structure. The origin of the heterogeneity observed with isolated reconstituted proteins is intriguing, and it is almost certainly multifactorial:

(i) *Static disorder*: There may be a range of conformations close to the minimum energy state that are stable on the timescale of the AFM measurement (ca. 10 s).
(ii) *Dynamic disorder*: Thermal fluctuations can produce short-lived changes in conformation, which may occur on the timescale of stochastic channel open states (ms or shorter). In this case the

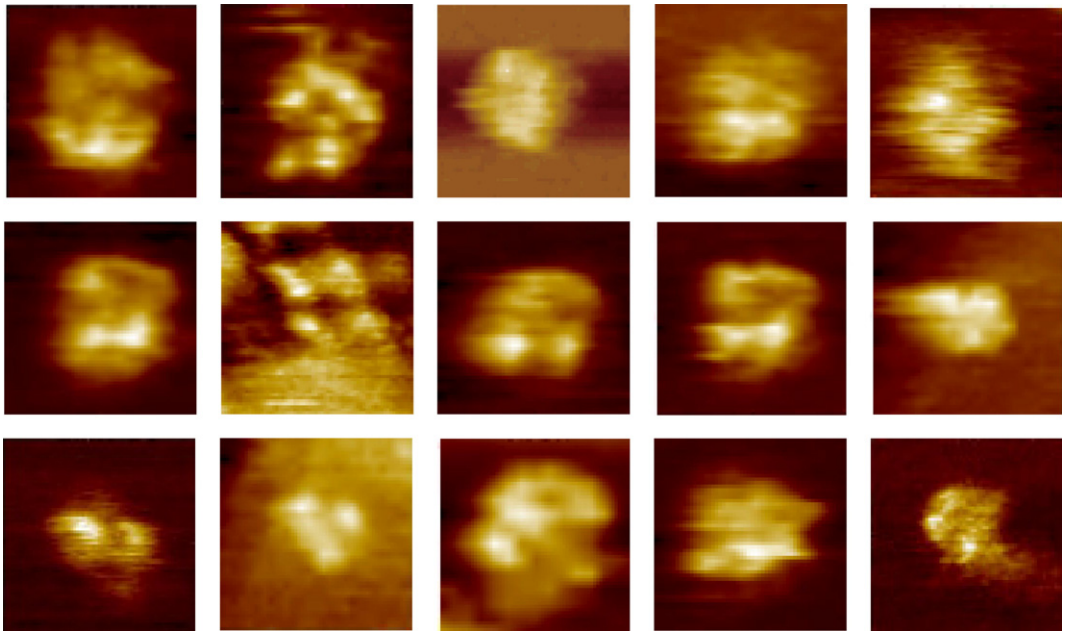

Fig. 6. AFM images (100 × 100 nm) of reconstituted AMPA-R indicating a range of different shapes. Most of the images contained several small features. Some contains four or more features, and some did not show distinctive features.

AFM images would represent a time-average of such structural fluctuations.

(iii) *Substrate interaction*: The membrane is weakly localized at the mica substrate, and any residual protein–substrate interaction could perturb the protein configuration. However, the relatively thick water layer between the bilayer and the substrate should greatly reduce this effect. The C-terminal domain could in principle make contact with the substrate, but there is no evidence of membrane curvature in the neighborhood of the receptor that such contact would inevitably induce.

(iv) *Tip–protein interaction*: The flexible linkers connecting the extracellular domains, and indeed the large flexible domains themselves, might distort under the stress applied by the cantilever tip. This effect is minimized in the experiments by employing soft cantilevers, but it cannot be entirely excluded.

Possibly the most surprising result of our AFM study is that the height of the extracellular domains above the bilayer surface is at most 2 nm. The cryo-EM data of Madden and co-workers for over-expressed homomeric GluR2 protein indicate that the extracellular domain extends 12 nm above the TMD [21,22]. Nakagawa et al. studied hetero-tetrameric AMPA-R purified from rat brains and obtained quite different results: two distinct structural type were identified – one with an extended extracellular configuration measuring 11 nm above the TMD, the second being a distinctly splayed structure in which the NTD dimers are well separated: considerable heterogeneity is observed in the latter case, and the height of the extracellular domains can be as small as 4–5 nm, essentially the height of the LBD [23]. The source of the disagreement between EM measurements is not understood at present. It may be that the protein itself – native (probably heteromeric) versus expressed (homomeric) – exists in different folded configurations, or it may be due to differences in sample preparation.

The small height measured in AFM may be due in part to tip-protein interaction causing the protein to be driven deeper into the membrane. However, comparing the AFM data and the EM measurements we see that the receptor volume is quite similar in the case of the over-expressed samples, assuming that we observed four extracellular domains whose diameters were 16 nm and heights were 2 nm in AFM, and assuming that extracellular domains were ellipsoid whose diameters were 14, 12, 11 nm in EM [22].

The tentative conclusion to be drawn from these measurements is that AMPA-R is highly deformable, due in part to the flexible inter-domain linkers but also because the extracellular domains are spatially unconfined in the membrane environment, unlike crystalline or low temperature environments. It will be important to extend AFM measurements to native receptors and to evaluate the impact of different sample preparation techniques on receptor configuration. A better understanding of receptor flexibility could be important in improving the reliability of screening techniques for finding lead candidates in drug development. In this regard work is now in progress to study glutamate binding as well as visualizing real time conformational changes using high-speed AFM. AFM might also be useful to examine the allosteric change of the AMPA-R through the cytoplasmic domain because of its key role in allosteric modulation by various proteins such as calmodulin, protein kinases and phosphatases [12]. The C-terminal domain also connects *in vivo* to the cytoskeleton in the postsynaptic terminal, and is strongly implicated in trafficking properties of AMPA-R such as internalization and recycling, which relate to synaptic plasticity. Consequently, AFM might also be used to examine the AMPA-R synaptic density, and ultimately to probe the mechanism of synaptic plasticity.

Acknowledgments

This research was funded partly by the Japan Society for the Promotion Science (JSPS) and the UK Bionanotechnology IRC. The authors thank Drs. Toru Ide and Yuko Takeuchi and Ms. Minako Hirano, Graduate School of Frontier Biosciences, Osaka University, for helpful suggestions on the electrophysiological measurements. The authors also thank K. Sumitomo and Y. Shinozaki and members of NTT Basic Research Laboratories for fruitful discussions, and Jelena Baranovic for helpful comments on the manuscript.

References

[1] D.G. Nicholls, Proteins, Transmitters and Synapses, Blackwell Science Limited, Oxford, UK, 1994.
[2] J.G. Nicholls, A.R. Martin, B.G. Wallace, From neuron to brain: a cellular and molecular approach to the function of the nervous system, 3rd edit, Sinauer Associates Inc, Sunderland, MA, USA, 1992.

[3] D.L. Small, C.L. Murray, R. Monette, S. Kawasaki-Yatsugi, P. Morley, Neuroprotective effects of a novel AMPA receptor antagonist, YM872, NeuroReport 9 (1998) 1261–1265.
[4] T. Namba, K. Morimoto, K. Sato, N. Yamada, S. Kuroda, Antiepileptogenic and anticonvulsant effects of NBQX, a selective AMPA receptor antagonist, in the rat kindling model of epilepsy, Brain Res. 638 (1993) 36–44.
[5] A.L. Drapalski, B.R. Ross, R.R. Peebles, B.L. Schwartz, C.L. Marvel, S.I. Deutsch, Topiramate improves deficit symptoms in a patient with schizophrenia when added to a stable regimen of antipsychotic medication, Clin. Neuropharmacol. 24 (2001) 290–294.
[6] T. Smith, A. Groom, B. Zhu, L. Turski, Autoimmune encephalomyelitis ameliorated by AMPA antagonists, Nat. Med. 6 (2000) 62–66.
[7] C. Sang, N. Ramadan, R. Wallihan, et al., LY293558, a novel AMPA/GluR5 antagonist, is efficacious and well-tolerated in acute migraine, Cephalalgia 24 (2004) 596–602.
[8] G.L. Collingridge, J.T.R. Isaac, Y.T. Wang, Receptor trafficking and synaptic plasticity, Nat. Rev. Neurosci. 5 (2004) 952–962.
[9] V.A. Derkach, M.C. Oh, E.S. Guire, T.R. Soderling, Regulatory mechanisms of AMPA receptors in synaptic plasticity, Nat. Rev. Neurosci. 8 (2007) 101–113.
[10] S.-H. Shi, Y. Hayashi, J.A. Esteban, R. Malinow, Subunit-specific rules governing AMPA receptor trafficking to synapses in hippocampal pyramidal neurons, Cell 105 (2001) 331–343.
[11] B.J. Hall, A. Ghosh, Regulation of AMPA receptor recruitment at developing synapses, Trends Neurosci. 31 (2008) 82–89.
[12] M.L. Mayer, Glutamate receptors at atomic resolution, Nature 440 (2006) 456–462.
[13] L.P. Wollmuth, A.I. Sobolevsky, Structure and gating of the glutamate receptor ion channel, Trends Neurosci. 27 (2004) 321–328.
[14] K.M. Partin, M.W. Fleck, M.L. Mayer, AMPA receptor flip/flop mutants affecting deactivation, desensitization, and modulation by cyclothiazide, aniracetam, and thiocyanate, J. Neurosci. 16 (1996) 6634–6647.
[15] G.-Q. Chen, E. Gouraux, Overexpression of a glutamate receptor (GluR2) ligand binding domain in *Escherichia coli*: application of a novel protein folding screen, Proc. Natl. Acad. Sci. U. S. A. 94 (1997) 13431–13436.
[16] M. Arvola, K. Keinanen, Characterization of the ligand-binding domains of glutamate receptor (GluR)-B and GluR-D subunits expressed in *Escherichia coli* as periplasmic proteins, J. Biol. Chem. 271 (1996) 15527–15532.
[17] N. Armstrong, Y. Sun, G.-Q. Chen, E. Gouaux, Structure of a glutamate receptor ligand-binding core in complex with kainate, Nature 395 (1998) 913–917.
[18] C. Rosenmund, Y. Stern-Bach, C.F. Stevens, The tetrameric structure of a glutamate receptor channel, Science 280 (1998) 1596–1599.
[19] G. Ayalon, Y. Stern-Bach, Functional assembly of AMPA and Kainate receptors is mediated by several discrete protein-protein interactions, Neuron 31 (2001) 103–113.
[20] A.I. Sobolevsky, M.V. Yelshansky, L.P. Wollmuth, The outer pore of the glutamate receptor channel has 2-fold rotational symmetry, Neuron 41 (2004) 367–378.
[21] M. Safferling, W. Tichelaar, G.n. Kümmerle, et al., First images of a glutamate receptor ion channel: oligomeric state and molecular dimensions of GluRB homomers, Biochemistry 40 (2001) 13948–13953.
[22] W. Tichelaar, M. Safferling, K. Keinänen, H. Stark, D.R. Madden, The three-dimensional structure of an ionotropic glutamate receptor reveals a dimer-of-dimers assembly, J. Mol. Biol. 344 (2004) 435–442.
[23] T. Nakagawa, Y. Cheng, E. Ramm, M. Sheng, T. Walz, Structure and different conformational states of native AMPA receptor complexes, Nature 433 (2005) 545–549.
[24] A. Engel, D.J. Müller, Observing single biomolecules at work with the atomic force microscope, Nat. Struct. Biol. 7 (2000) 715–718.
[25] S. Kasas, N.H. Thomson, B.L. Smith, et al., Escherichia coli RNA polymerase activity observed using atomic force microscopy, Biochemistry 36 (1997) 461–468.
[26] W. Suhara, M. Kobayashi, H. Sagara, et al., Visualization of inositol 1,4,5-trisphosphate receptor by atomic force microscopy, Neurosci. Lett. 391 (2006) 102–107.
[27] T. Vaithianathan, K. Matthias, B. Bahr, et al., Neural cell adhesion molecule-associated polysialic acid potentiates alpha-amino-3-hydroxy-5-methylisoxazole-4-propionic acid receptor currents, J. Biol. Chem. 279 (2004) 47975–47984.
[28] T. Ide, T. Yanagida, An artificial lipid bilayer formed on an agarose-coated glass for simultaneous electrical and optical measurement of single Ion channels, Biochem. Biophys. Res. Commun. 265 (1999) 595–599.
[29] M. Hollmann, M. Hartley, S. Heinemann, Ca^{2+} permeability of KA-AMPA-gated glutamate receptor channels depends on subunit composition, Science 252 (1991) 851–853.
[30] H. Sprong, P.v.d. Sluijs, G.v. Meer, How proteins move lipids and lipids move proteins, Nat. Rev., Mol. Cell Biol. 2 (2001) 504–513.
[31] T.M. Bayer, M. Bloom, Physical properties of single phospholipid bilayers adsorbed to micro glass beads—a new vesicular model system studied by 2H-nuclear magnetic resonance, Biophys. J. 58 (1990) 357–362.
[32] J.F. Hainfeld, R.D. Powell, New frontiers in gold labeling, J. Histochem. Cytochem. 48 (2000) 417–480.
[33] J.M. Robinson, T. Takizawa, D.D. Vandré, Enhanced labeling efficiency using ultrasmall immunogold probes: immunocytochemistry, J. Histochem. Cytochem. 48 (2000) 487–492.
[34] N.R. Kramarcy, R. Sealdck, Commercial preparations of colloidal gold-antibody complexes frequently contain free active antibody, J. Histochem. Cytochem. 39 (1991) 37–39.
[35] J.L. Marx, Antibody structure: now in three dimensions, Science 189 (1975) 1075–1077.
[36] P.L.T.M. Frederix, M.R. Gullo, T. Akiyama, et al., Assessment of insulated conductive cantilevers for biology and electrochemistry, Nanotechnology 16 (2005) 997–1005.